# Evaluation of the Formability of AA2198-T3 Al-Li alloy in Warm Sheet Hydroforming

**Hui Wang**
College of Mechanical and Electrical Engineering, Nanjing University of Aeronautics and Astronautics, Nanjing 210016, P. R. China

**Sijia Cheng**
College of Mechanical and Electrical Engineering, Nanjing University of Aeronautics and Astronautics, Nanjing 210016, P. R. China

**Zhuang Ye** ( yezhuang1998@163.com )
Nanjing University of Aeronautics and Astronautics

**Tianli Wu**
College of Mechanical and Electrical Engineering, Nanjing University of Aeronautics and Astronautics, Nanjing 210016, P. R. China

**Kai Jin**
School of Materials Science and Engineering, Ocean University of China, Qingdao 266100, P. R. China

**Xunzhong Guo**
College of Material Science and Technology, Nanjing University of Aeronautics and Astronautics, Nanjing 211100, P. R. China

**Research Article**

**Keywords:** Al-Li alloy, formability, hydrodynamic deep drawing, GTN model, warm hydroforming, microstructure

**Posted Date:** April 19th, 2021

**DOI:** https://doi.org/10.21203/rs.3.rs-376565/v1



**Version of Record:** A version of this preprint was published at The International Journal of Advanced Manufacturing Technology on September 5th, 2021. See the published version at https://doi.org/10.1007/s00170-021-07961-z.

# Evaluation of the formability of AA2198-T3 Al-Li alloy in warm sheet hydroforming

Hui Wang [1], Sijia Cheng [1], Zhuang Ye [1],

Tianli Wu [1], Kai Jin [2], Xunzhong Guo [3]

*1. College of Mechanical and Electrical Engineering, Nanjing University of Aeronautics and Astronautics, Nanjing 210016, P. R. China*

*2 .School of Materials Science and Engineering, Ocean University of China, Qingdao 266100, P. R. China*

*3.College of Material Science and Technology, Nanjing University of Aeronautics and Astronautics, Nanjing 211100, P. R. China*

**Corresponding author:** Zhuang Ye; Tel : 18762327762; Email: yezhuang1998@163.com

## Abstract

This study aims to investigate the formability of the AA2198-T3 Al-Li alloy in hydrodynamic deep drawing (HMDD), through experimentation and finite element simulation. The effects of the most critical factors were studied: die cavity pressure and forming temperature. The Gurson−Tvergaard−Needleman model (GTN model) was employed to analyze the formability of AA2198-T3 Al-Li alloy and predict the fracture in the hydroforming of a cylindrical part. Both the numerical and experimental results showed that the increase of the pressure inside the liquid chamber, within a certain range, contributes to improve the formability of the alloy. Increasing the temperature would reduce the required pressure for sheet hydroforming. Notably, the appropriate chamber pressure was beneficial to form good quality parts with a relatively uniform wall thickness. By analyzing the fracture morphologies, the brittle fracture of AA2198-T3

plays a main role at room temperature, but the ductile fracture was shown at the elevated temperature.

**Keywords:** Al-Li alloy; formability; hydrodynamic deep drawing; GTN model; warm hydroforming; microstructure.

# Statement

I, on behalf of all the authors of the manuscript entitled "*Evaluation of the formability of AA2198-T3 Al-Li alloy in warm sheet hydroforming"*, declare that

1. No ethical approval is required for this article.

2. The article has been written by the stated authors who are all aware of its content and approve its submission.

3. The article has not been published previously and agree to release.

4. Contribution of the author:

Hui Wang: Put forward research ideas and design research schemes.

Sijia Cheng: Responsible for collecting, collating and analyzing data.

Zhuang Ye: Responsible for revision, typesetting and final revision.

Tianli Wu, Kai Jin, Xunzhong Guo: In charge of conducting experiments.

5. Funding for this article came from the Bureau of international cooperation of the Chinese Academy of Sciences (174321KYSB20150020), the National Natural Science Foundation of China (Grant No. 51605310), Jiangsu Province Science and Technology Program (Grant No. BE2016156), Shenyang Science and Technology Program (17-32-6-00), the Research Project of State Key Laboratory of Mechanical System and Vibration (MSV201708) and the Research Fund of Nanjing University of Aeronautics and Astronautics (No. YAH17019).

6. No conflict of interest exists, or if such conflict exists, the exact nature of the conflict

must be declared.

7. The data that support the findings of this study are available from the corresponding author upon reasonable request.

Signature

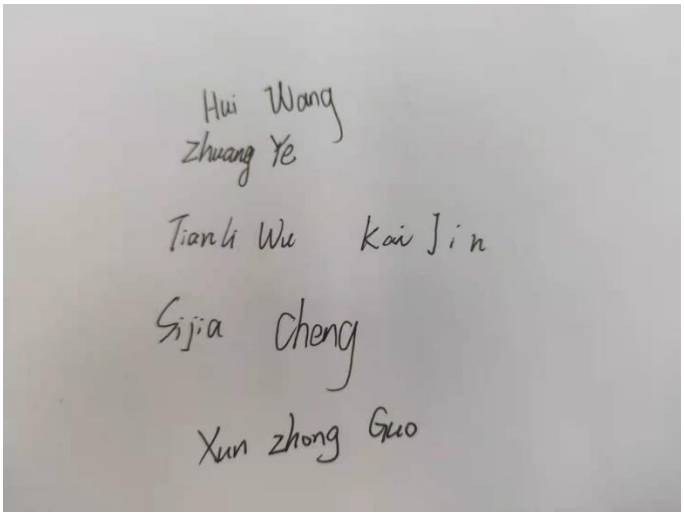


## 1. Introduction

With the rapid development of the aerospace industry, modern military and civilian aircraft have developed towards high-speed overload, long life and flight safety. The materials and weight requirements of aircraft structural parts have become increasingly stringent. Aluminum-lithium (Al-Li) alloys offer great superiority for use in aircraft structure since they reduce the density, increase stiffness, increase the resistance to fracture toughness and fatigue crack growth, and enhance the corrosion resistance [1,2]. With the addition of lithium, the weight (density) of the alloy reduces approximately 3% for each 1% lithium addition to aluminium, while Young's modulus increases about 6% [1,3].

AA2198-T3 Al-Li alloy, as the third generation of damage-tolerant Al-Li alloys, is considered as one of the most competitive lightweight and high strength structural materials in the aerospace industry [4-7]. However, the application of formed parts in

critical structures is still restricted by the material low formability at ambient temperature [8-10].

Owing to the technical advantages of high forming limit, high dimensional precision, and good surface quality, hydrodynamic deep drawing (HMDD) method is widely used in the forming of complex thin-walled parts, especially aluminium alloy parts used in the aerospace field [11,12]. In the process, filling chamber instead of the original die, the pressure on the sheet comes from the liquid medium instead of a rigid die, hydraulic pressure to promote the formation of sheet metal. Under the action of the liquid chamber pressure, the plate and the punch fit closely, and the friction effect reduces the tendency of the plate to break at the corner of the punch; at the same time, the radial tensile stress is effectively reduced, and the wall thickness uniformity of the plate is improved. In addition, when the pressure of the liquid chamber reaches a certain value, the hydraulic pressure lifts the sheet material, and the liquid can flow between the sheet material and the die and blank holder. The lubricated function reduces the deformation resistance of the flange and the friction between the sheet and the die, improving the surface quality of the part. However, the application of Al-Li alloy formed components in critical structures is still restricted, due to the low formability at room temperature. Warm hydroforming provides a good solution since the elevated temperature can increase the flow of the metal [13]. Fig. 1 shows a schematic representation of the warm HMDD process.

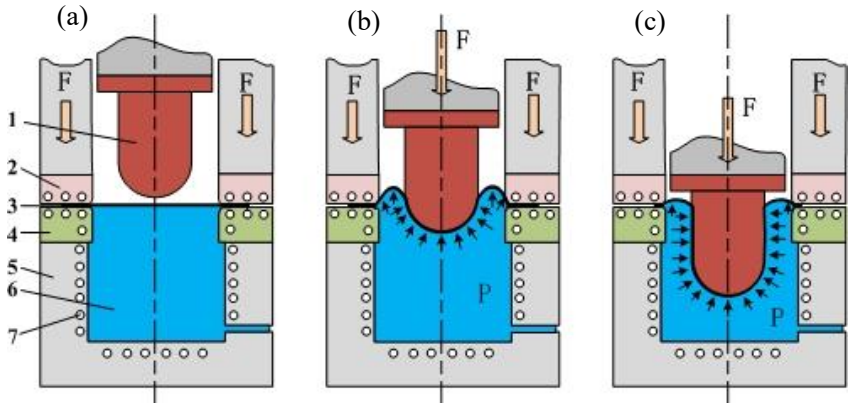


Fig.1 Schematic drawing of hydrodynamic deep drawing process: (a) Sheet in position and downward movement of blank holder; (b) Downward movement of punch; and (c) End of the

sheet forming; 1-punch; 2-blank holder; 3-sheet; 4-die; 5-liquid cavity; 6-liquid; 7-electrical heat rod

Currently, the researcher on the HMDD process mostly focus on the effects of process parameters at ambient temperature. Hama et al. [14] experimentally investigated the effect of the outflow volume of the pressure medium on the fluid-lubrication effect during the sheet hydroforming and concluded that the fluid-lubrication effect significantly affected the forming quality. Wang et al. [15] studied the blank shape and pressure-loading path on the AA2024 irregular box sheet hydroforming process, and they found that the part can be formed with the appropriate blank shape and die cavity pressure. In terms of sheet warm hydro-mechanical deep drawing, the material behavior of Al5754 was characterized using both tensile and hydraulic bulge tests under room and warm temperature conditions [16]. The results suggested that, in general, formability of AA5754 could be improved with high forming temperature (>200ºC). Hosseinpour et al. [17] investigated the formability of AA5052 in warm hydrodynamic deep drawing. They demonstrated that the thickness distribution could be improved by increasing the maximum oil pressure to a certain level, leading to the increase of the punch force. Ling et al. [18] verified the forming parameters of sheet hydro-mechanical deep drawing on AA2198-T3 alloy by numerical simulation at room temperature. However, few studies investigated the solutions to improve the formability of Al-Li alloy in the warm hydroforming.

Therefore, the subject of the present paper was to study the characteristic of plastic deformation of AA2198-T3 alloy in the warm hydroforming. Meanwhile, the effect of the process parameters on the fracture behavior in the hydroforming process was numerically studied, employing the GTN model.

## 2. Experimental

### 2.1. Uniaxial tensile tests

Uniaxial tensile tests were conducted on a STM5000 testing machine. The sheet

specimens of AA2198-T3 Al-Li alloy with the thickness of 2.0 mm were cut along the rolling direction. The deformation behavior at ambient temperature and 423K were measured under the strain rates of $10^{-3}s^{-1}$, $10^{-2}s^{-1}$ and $10^{-1}s^{-1}$. Considering the effect of strain and strain rate on the flow stress of the material, Fields-Backofen [19] constitutive equation is often used to describe the stress-strain relationship of materials under different deformation temperatures and different strain rates. The parameters of the Fields-Backofen equation shown in Equation (1) are obtained through isothermal experimental testing. Parameter fits and is listed in Table 1.

$$\sigma = K\varepsilon^{n}\dot{\varepsilon}^{m} \tag{1}$$

where K is strength coefficient, n is hardening exponent and m is the strain rate sensitivity exponent.

In the equation, K, n and m are constants of the material at a certain strain rate and a certain deformation temperature, that is, the values of K, n and m will change with the changes of temperature and strain rate. K, n, m and strain rate and temperature T mathematical relationship.

The hardening exponent-n is as followed.

$$n = \frac{\partial \ln\sigma}{\partial \ln\varepsilon}\bigg|_{\dot{\varepsilon},T} \tag{2}$$

From the deduced formula, it can be found that at a certain temperature and a certain strain rate, the strain hardening exponent n is the slope of the straight line in the $\ln\varepsilon - \ln\sigma$ coordinate plane. The stress-strain logarithmic relationship curves at different strain rates were made for each temperature. Take the plastic deformation stage curve fitting to obtain a straight line, and find the slope of the straight line, that is, the hardening exponent n.

The strain rate sensitivity exponent-m is as followed.

$$m = \frac{\partial \ln\sigma}{\partial \ln\dot{\varepsilon}}\bigg|_{\varepsilon,T} \tag{3}$$

The strain rate sensitivity exponent-m was determined using a constant strain rate stretching method. At a certain temperature, stress-strain curves obtained at different strain rates are plotted in the same coordinate system. Select the uniform plastic stage, obtain the stress-strain coordinate point and take the natural logarithm, draw the coordinate points in the same coordinate system and perform linear regression fitting to obtain the curve. The slope of the straight line is the m value at the temperature.

Strength coefficient-K

$$K = \frac{\sigma}{\varepsilon^{n} \dot{\varepsilon}^{m}} \tag{4}$$

The strength coefficient K at each temperature was determined from the calculated values of m and n, respectively.

Table 1. Material parameters of AA2198-T3

| *T* | *K* | *n* | *m* |
|---|---|---|---|
| **298K** | 737.51 | 0.375 | 0.0019 |
| **423K** | 476.55 | 0.266 | 0.0058 |

## 2.2. Sheet hydroforming tests

Hydrodynamic deep drawing experiments were carried out to evaluate the formability of AA2198-T3 Al-Li alloy in warm sheet hydroforming at the double-action hydraulic press. The diameter and thickness of the initial sheet blank was 127.6 mm and 2.0 mm. The fillet radius of punch and die were 10 mm and 8 mm respectively. The blank holder gap was 1.1 times the sheet thickness. Fig. 2 shows the experiment equipment of the warm HMDD.

Firstly, the liquid cavity was fully filled with hydraulic oil under high temperature (≤573K). Then, the sheets were put on the die surface and the blank holder gap was kept fixed, at 2.2 mm, through walking beam of the double-action hydraulic press. By heating the tools and the hydraulic oil, the sheet reached the required temperature. The

punch started the downward movement, to press the sheet into the cavity, once the temperature indicator reach the required value, and the pressure of the liquid chamber was controlled by using the pressure control valve.

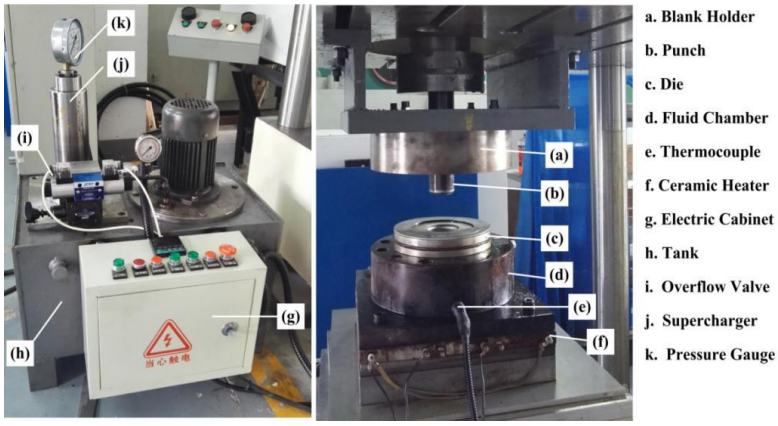


Fig. 2 The experiment equipment of the warm HMDD

The appropriate hydraulic pressure of liquid in the hydrodynamic chamber is one of the key factors that determine the success of HMDD process. Due to the action of pressure inside the liquid chamber, the sheet was lifted upwards. Then, the liquid flowed into the gap between the sheet and the die so that the effective lubrication was obtained and the frictional resistance decreased. Furthermore, because of the action of hydraulic pressure, the sheet was attached to the punch closely. The loading paths of hydraulic pressures at different temperatures is shown in Fig. 3a. As the punch is slowly depressed, the hydraulic value increases linearly and remains constant when the hydraulic pressure reaches a suitable value until the drawing deformation is completed.

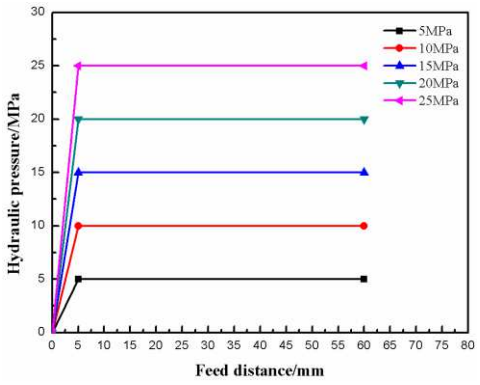


Fig. 3.a The loading paths of hydraulic pressures

## 3. Numerical simulation

### 3.1. GTN damage model

Based on the microscopic void theory, the fracture of metals includes three stages, namely void nucleation, void growth, and void coalescence [20]. Gurson [21] proposed a continuum damage model according to the theory. The yield condition is shown as follows:

$$\Phi = \left(\frac{q}{\sigma_y}\right) + 2f^* q_1 \cosh\left(-q_2 \frac{3p}{2\sigma_y}\right) - \left(1 + q_3 f^{*2}\right) = 0 \tag{5}$$

where q is the macroscopic von Mises equivalent stress, $\sigma_y$ is the current flow stress of the matrix, p is the macroscopic hydrostatic stress, and the function $f^*(f)$ models the rapid loss of stress carrying capacity, which accompanies the void coalescence. This function is defined in terms of the void volume fraction as follows:

$$f^* = \begin{cases} f & \text{if} \quad f \leq f_c \\ f_c + \frac{\bar{f}_F - f_c}{f_F - f_c}(f - f_c) & \text{if} \quad f_c < f < f_F \\ \bar{f}_F & \text{if} \quad f \geq f_F \end{cases} \tag{6}$$

$$\bar{f}_F = \frac{q_1 + \sqrt{q_1^2 - q_3}}{q_3} \tag{7}$$

In the above relationship, $f_c$ is a critical value of the void volume fraction, and $f_F$ is the value of void volume fraction at which there is a complete loss of stress carrying capacity in the material.

Damage evolution in the metal includes two stages, void growth $f_g$ and nucleation $f_n$:

$$\dot{f} = \dot{f}_g + \dot{f}_n \tag{8}$$

The growth of the existing voids is based on the law of conservation of mass and is expressed in terms of the void volume fraction:

$$\dot{f}_g = (1-f)\dot{\varepsilon}^p_{kk} \tag{9}$$

where $\dot{\varepsilon}^{p}_{kk}$ is hydrostatic component of the plastic strain rate tensor.

The nucleation of voids is given by a strain-controlled relationship:

$$\dot{f}_n = A\dot{\varepsilon}^p_e \tag{10}$$

$$A = \frac{f_N}{S_N\sqrt{2\pi}} \exp\left[-\frac{1}{2}\left(\frac{\varepsilon^p_e - \varepsilon_N}{S_N}\right)^2\right] \tag{11}$$

where $f_N$ is the volume fraction of the nucleated voids and voids are nucleated only in tension. The normal distribution of the nucleation strain has a mean value $\varepsilon_N$ and standard deviation $S_N$, $\varepsilon^{p}_{e}$ is the von Mises equivalent plastic strain, and $\dot{\varepsilon}^{p}_{e}$ is the von Mises equivalent plastic strain rate.

According to the recommendations found in the literature of Needleman and Tvergaard [22] and Benseddiq and Imad [23], the values of some parameters in the present study have been adopted as follows: $q_1 = 1.5$, $q_2 = 1$, $q_3 = {q_1}^2 = 2.25$, $S_N$=0.1 and $\varepsilon_N = 0.1$. The remaining parameters, $f_0$, $f_N$, $f_c$ and $f_F$ are very difficult to be directly evaluated from the experimental tests. However, an inverse finite element approach was adopted in the present work to determine the proper values of $f_0$, $f_N$, $f_c$ and $f_F$ [24-26]. The tensile test of AA2198-T3 alloy specimen have been simulated using Abaqus finite element code. Consequently, the parameters of GTN model for AA2198-T3 at different temperatures were obtained as shown in Table 2.

Table 2. GTN model parameters for AA2198-T3 at different temperatures

| | $q_1$ | $q_2$ | $q_3$ | $f_0$ | $f_N$ | $S_N$ | $\varepsilon_N$ | $f_c$ | $f_F$ |
|---|---|---|---|---|---|---|---|---|---|
| **298k** | 1.5 | 1.0 | 2.25 | 0.0016 | 0.02 | 0.1 | 0.1 | 0.024 | 0.15 |
| **423k** | 1.5 | 1.0 | 2.25 | 0.002 | 0.0214 | 0.1 | 0.1 | 0.095 | 0.40 |

### 3.2. Finite element model

First of all, combined with the GTN model and Fields-Backofen equation as shown in

Eq. (1), the engineering stress-strain curves of uniaxial tension for AA2198-T3 Al-Li alloy can be obtained from FE simulation, which were compared with those from experiments as shown in Fig. 3b. It can be seen that the parameters used are suitable in the FE simulation of the uniaxial tensile test.

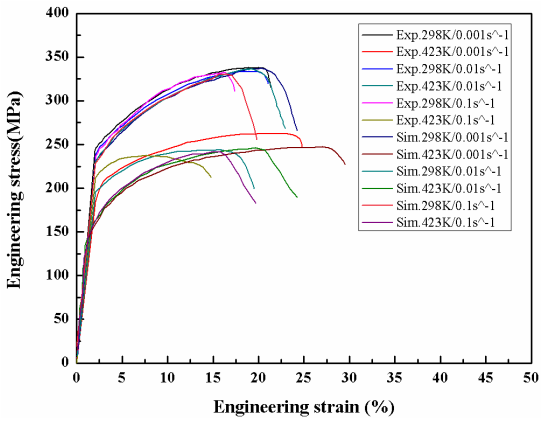


Fig. 3.b Engineering stress-strain curves of AA2198-T3 Al-Li Alloy obtained from experiments and simulation

In order to simulate the warm sheet hydroforming, a model for the processes was built on Abaqus/Explicit. By considering the symmetry of the process, a 3D elasto-plastic model with only a quarter part of the sheet and the dies was established to improve the calculation efficiency, as illustrated in Fig. 4a. The blank holder has a fillet radius of 6mm. The gap between blank holder and punch is maintained at 2mm， and the gap between punch and die is kept constant at 3mm. The diameters of punch and die are 58mm and 64mm, respectively.

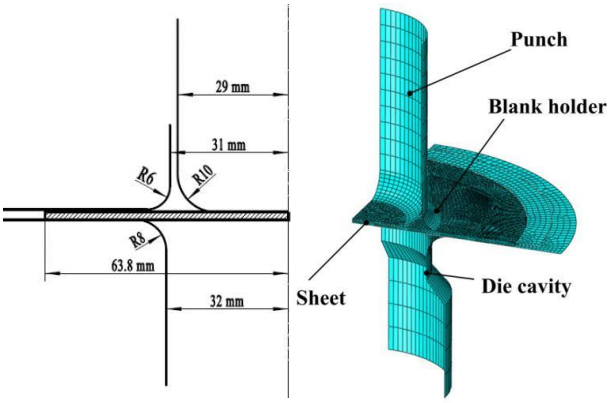


Fig. 4.a The finite element model and dimensions of tools.

The symmetry boundary conditions were assigned to the edges of the sheet. The sheet was discretized with C3D8R solid element and tools used discrete rigid shell elements. The gap between the blank holder and the die is 1.1 the sheet initial thickness and the punch speed is 15.0 mm/s. The Coulomb friction law was used to define the contact conditions. Since there is hydraulic oil between the sheet and the die surface and grease was applied to the blank holder for lubrication, the friction coefficients at the sheet/die, sheet/blank holder, and sheet/punch interfaces were assumed as 0.05. The discrete rigid dies should be meshed finely at the position in contact with the sheet, such as punch corner and die corner for accurate results. As the same as the experiments, 0, 5.0 MPa, 10.0 MPa, 15.0 MPa, 20.0 MPa and 25.0 MPa were chosen as the hydraulic pressures at 298 K and 423 K to evaluate the effect of hydraulic pressure inside liquid chamber on the thickness distribution.

## 4. Results and discussion

### 4.1 Deformation behavior and formability

The distribution of the equivalent plastic strain predicted by the FE simulation model under different hydraulic pressures at 298 K and 423 K are depicted in Figs. 4b and 4c respectively. The fracture occurred on punch corner or cylinder wall, when the pressure is not enough. Hydraulic anti-expansion can effectively prevent wrinkling of the sheet material at the corners of the die, and plays an important role in improving the forming accuracy of the part and increasing the forming limit of the sheet.

The formability at the room temperature can be improved as hydraulic pressure increases but still hard to form a completed cylindrical part as shown in Fig. 5. However, in warm hydroforming conditions it is easier to obtain good quality components, compared with forming at room temperature as shown in Fig. 5. The maximum draw depth was 35.4 mm at 298 k. Since the depth of the cylindrical part was not increased

too much, the hydraulic pressure does not play a big role at the room temperature. As depicted in Fig. 4b, it can be seen clearly that the fracture occurred at the wall where high uniaxial tensile stress exists. It is difficult to draw a cylindrical part without cavity pressure. In other words, conventional deep drawing is not suitable for AA2198-T3 alloy.

When the forming temperature of 423 K was utilized during the process of HMDD, it is obviously seen in Fig. 4c that the elevated temperature improved the formability of the AA2198-T3. A completed cylindrical part was formed at the hydraulic pressure of 25.0 MPa with a depth of 58.15mm. This can be verified by the GTN model and the void volume fraction (Fig. 12). When the liquid temperature rises from 298 K to 423 K, the void volume fraction fracture limit increases from 0.04 to 0.067. Therefore, the hydraulic drawing limit of AA2198-T3 Al-Li alloy increases. Besides, as shown in Fig. 5，at 298 K, the drawing depth has a significant increase when the hydraulic pressure is in the range of 15 MPa-20 MPa. At the condition of 423 K, the drawing depth has a significant increase when the hydraulic pressure is in the range of 20 MPa-25 MPa.

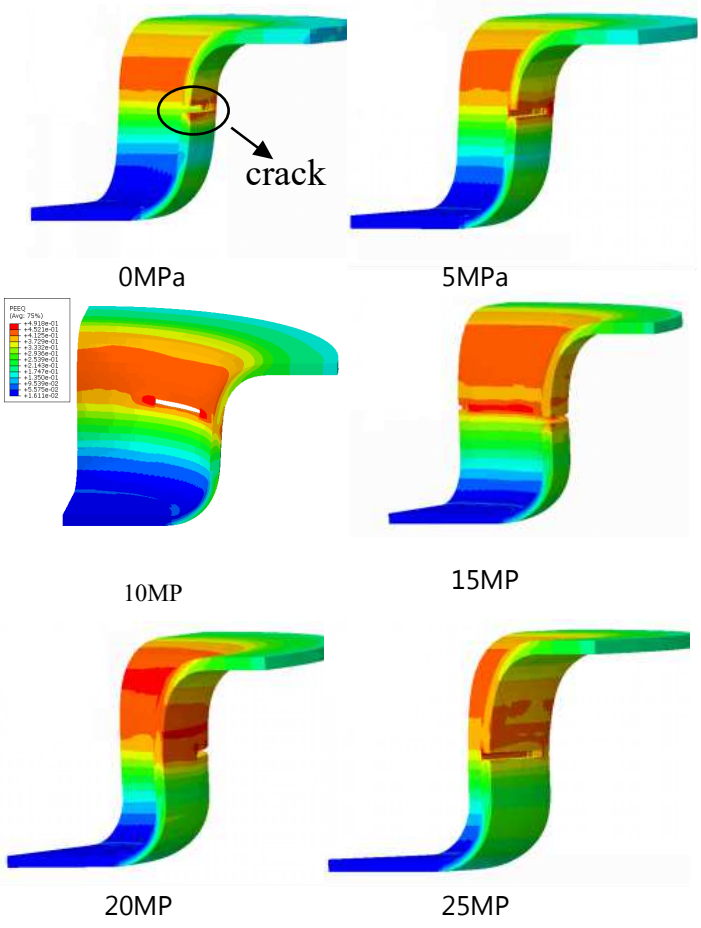

Fig. 4.b Plastic strain distributions and fracture under different hydraulic pressures at 298K.

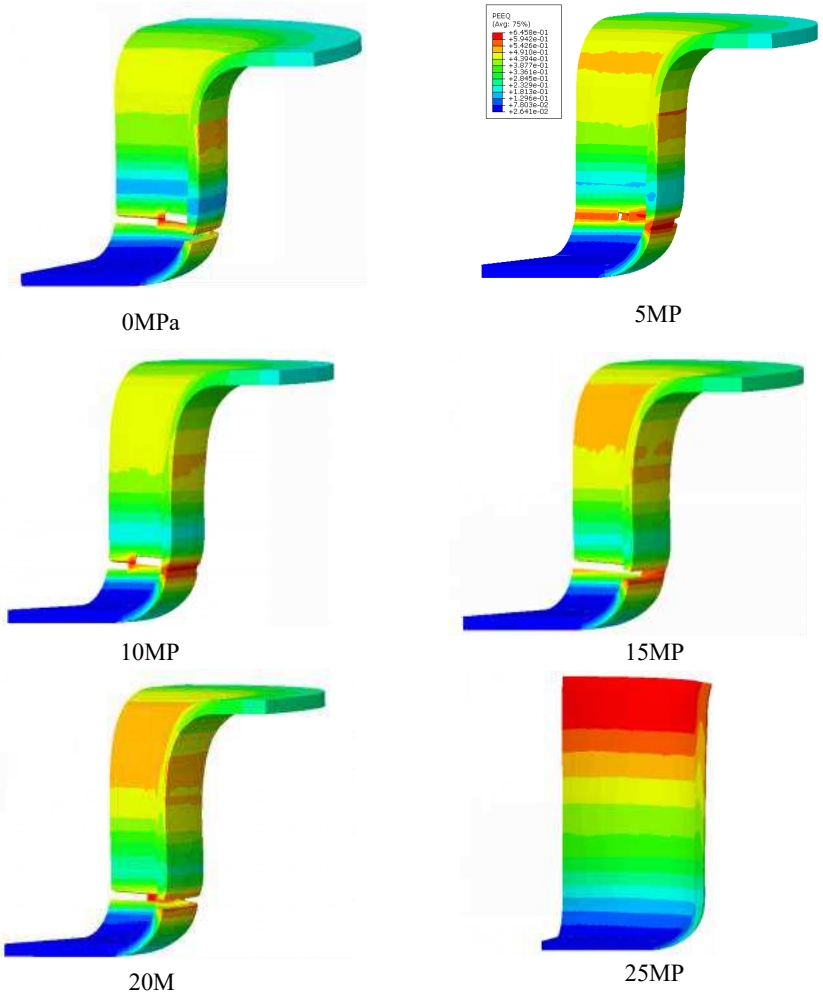


Fig. 4.c Plastic strain distributions and fracture under different hydraulic pressures at 423K.

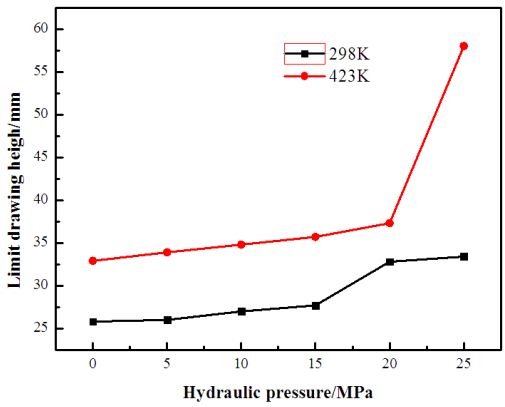


Fig. 5 The limit drawing height at different hydraulic pressures.

In addition, the thickness distributions under different hydraulic pressures are

shown in Fig. 6. With the increase of hydraulic pressure, the thickness distribution becomes nonuniform. In zone I, the thickness distribution is relatively uniform. In zone II, the overall thickness distribution is not uniform, and the thickness variation is large; however, with the increase of hydraulic pressure, the thickness change amplitude decreases; at 25 MPa, the thickness distribution at 423 K is more uniform than 298 K. In zone III, the thickness increased obviously as true distance form the cup center increased, and the thickness of the 25 MPa was the smallest. The thickness at the bottom of the cup (zone I) is approximately constant at 298 K and 423 K. The thickness at the bottom becomes increasingly closer to initial thickness with the increase of hydraulic pressure, due to the equal biaxial stretching. At zone II including punch corner and cup wall, the sheet experiences more thickness reduction and the fracture is likely to occur in this region. The thickness of the flange increases due to the compression stress state in the circumferential direction. This effect is visible in zone III, where wrinkling might also occur.

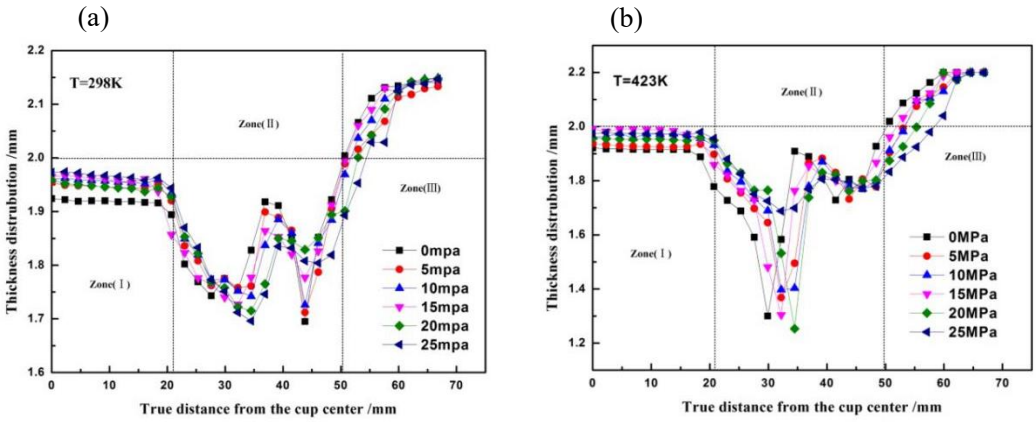


Fig. 6 Thickness distribution of the formed parts achieved at the maximum height under different hydraulic pressures: (a) 298K, (b) 423K.

The formed parts obtained from the HMDD experiment are shown in Fig. 7. The cylindrical part cannot be formed completely at the room temperature by using the HMDD. However, hydraulic pressure could improve the depth. The elevated temperature would improve the formability at 25 MPa hydraulic pressure since the deformation resistance of the blank flange decreases, which favors the material flow. Comparing with the experimental results, the fracture generated from FE simulation at

zone II is consistent.

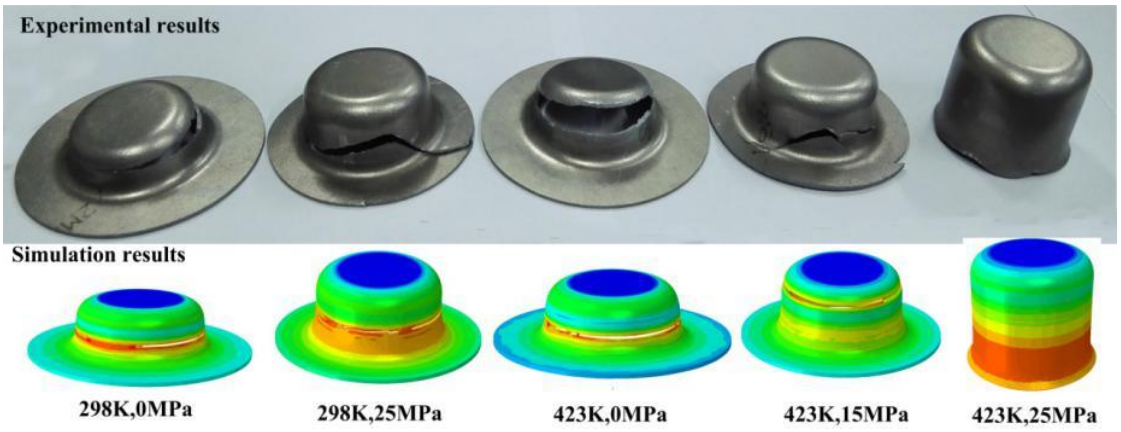


Fig. 7 Comparison between experimental and simulation results.

Fig. 8 illustrates the thinning ratio obtained from simulation and experiment for 25 MPa at 298 K and 423 K. The thickness distribution obtained from FE simulation are very close to experimental results. The thickness distribution at 423 K is more uniform than that at the room temperature. The punch force during the process with the hydraulic pressure of 25 MPa is depicted in Fig. 9. The force for warm HMDD is much lower than that for cold HMDD. In addition, the actual drawing force was greater than that obtained from FE analysis, which may be caused by friction between punch and seal ring on blank holder.

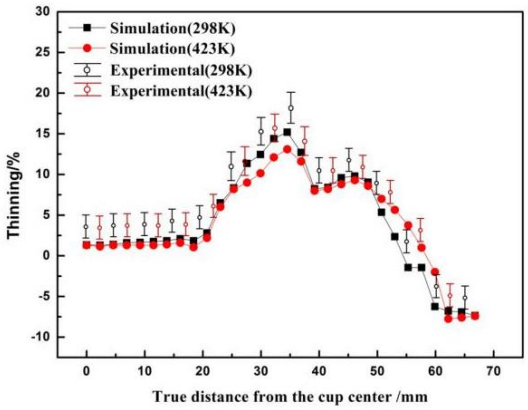


Fig. 8 Thinning ratio of the formed part at the hydraulic pressure of 25 MPa

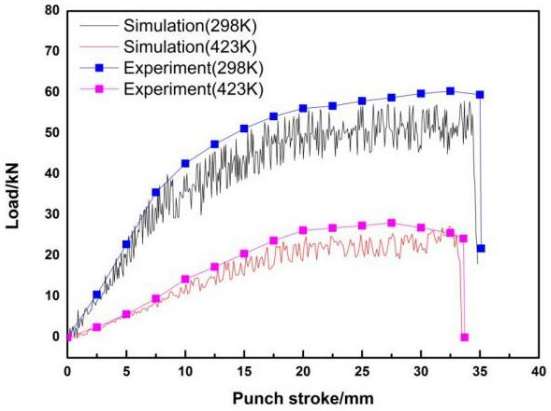


Fig. 9 The comparison of punch force of simulation and experiment with the hydraulic pressure of 25 MPa

The formability of AA2198-T3 Al-Li alloy is not good at room temperature. The HMDD process with proper fluid pressure can improve the formability of the alloy. The formed depth promoted with the increase of hydraulic pressure, but there is an optimal hydraulic pressure value beyond which the sheet will wrinkle. The fracture will occur after the pressure is up to a certain value at room temperature.

By utilizing the warm HMDD, the formability of A2198-T3 Al-Li alloy was much improved at the elevated temperature (423 K). The hydraulic pressure has a significant influence on the warm HMDD. When the hydraulic pressure reached a certain value (25 MPa), the formability is higher. Besides, the thickness distribution is more uniform at 423 K than at room temperature.

### 4.2. Microstructure and fracture mechanism

The microstructure and fracture of AA2198-T3 Al-Li alloy after HMDD was observed by Hitachi TM-3000 Tabletop Scanning Electron Microscope. SEM specimens were cut from the fracture region of the part at different temperatures with 15MPa.

From the SEM images in Fig. 10 (a), there is a large and smooth micro-fracture surface with a few dimples. At the high magnification (Fig. 11(a)), the dimples barely exist. Therefore, the brittle fracture plays a dominant role at room temperature, appearing the poor ductility.

Meanwhile, at the elevated temperature of 423 K, the micro-fracture surface

presents a fibrous structure in Fig. 10 (b) which is a typical characteristic of ductile fracture. Furthermore, many dimples and a large number of voids appear in the micro-fracture surface that demonstrate good plasticity as shown in Fig. 11 (b). The deformation should be the result of the combined action of grain deformation, grain dislocation movement and grain boundary movement. When the action cannot be eliminated, stress concentration will be generated. At this moment, micro-voids will appear in the grain boundary. As micro-voids coalesce together, the ductile fracture begins to initiate. Besides, the distribution of dimples is uneven and the dimples are small and shallow. With the increase of temperature, dimples increase and become more homogeneous.

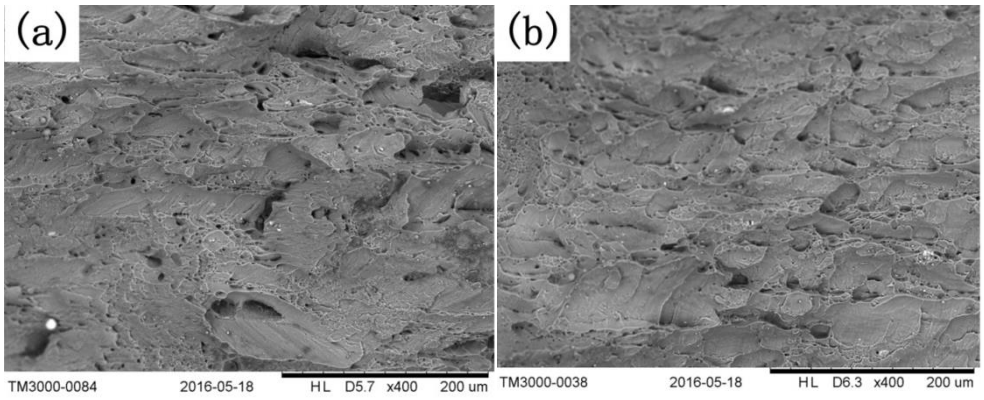


Fig. 10 Fracture microstructure at low magnification (×400) in different temperatures: (a) 298K; (b) 423K

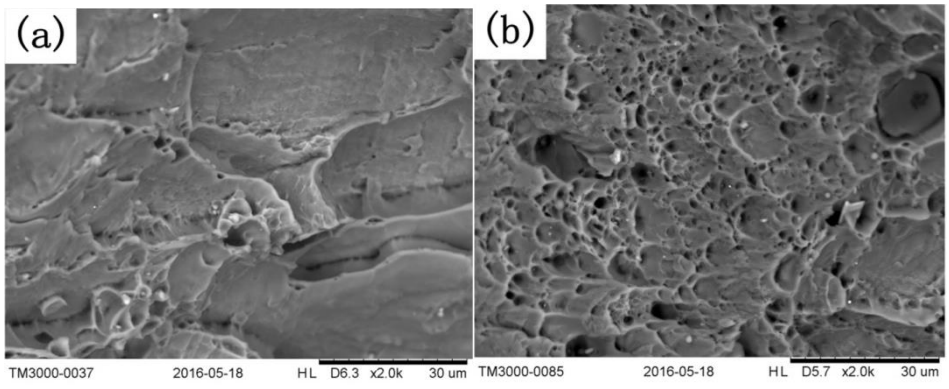


Fig. 11 Fracture microstructure at high magnification (×2000) in different temperatures: (a) 298K; (b) 423K

When the hydraulic pressure is 15 MPa, the void volume fraction at 298 K and 423 K were shown in Fig.12. At 298 K, when the pore volume fraction reaches 0.147,

near the ultimate fracture void volume fraction of 0.15, the AA2198-T3 Al-Li alloy begins to break. This is consistent with the parameters of the GTN model shown in Table 2. However, with the liquid temperature rises to 423 K, the ultimate fracture value of the void volume fraction increases to 0.4, the material will fracture. As the liquid temperature rises, the fracture limit of the void volume fraction also increases. Therefore, the forming depth of AA2198-T3 Al-Li alloy is also significantly increased. From the void volume fraction, it can be seen that the fracture is likely to occur at punch corner or cylinder wall of the product, which is consistent with the results of the plastic strain cloud diagram.

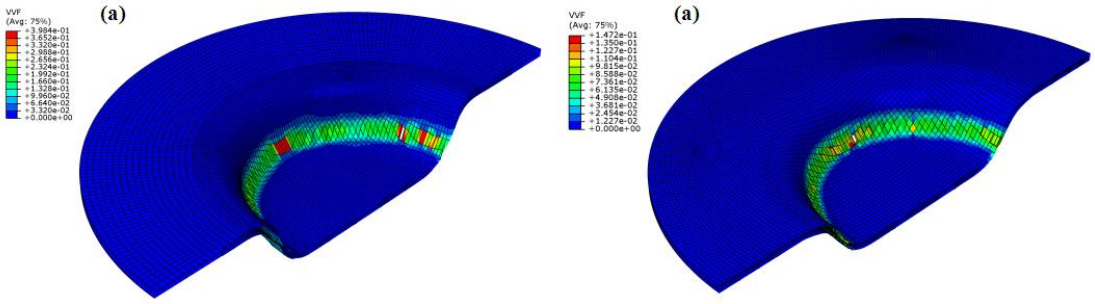


Fig. 12 void volume fraction at different temperatures: (a) 423K, (b)298k

By analyzing the SEM images, the brittle fracture of AA2198-T3 Al-Li alloy plays a main role at the room temperature. The ductile fracture was shown at the elevated temperature. The GTN model can reflect the fracture behavior through calculating void nucleation (Fig. 13) and void growth (Fig. 14), which can be confirmed by the SEM images of AA2198-T3.

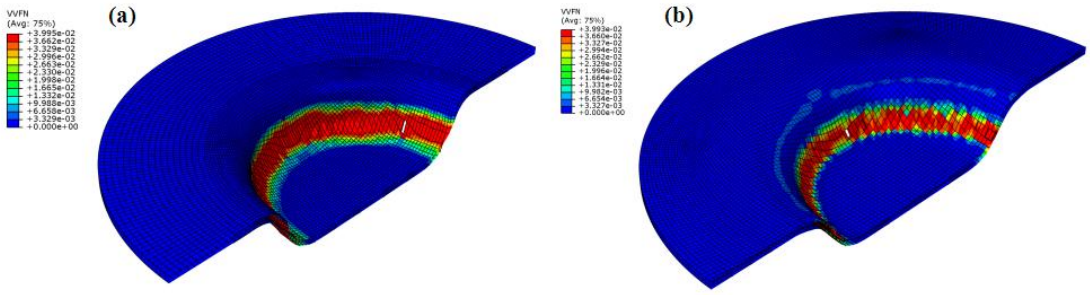


Fig. 13 void volume fraction due to nucleation at different temperatures: (a)423K, (b)298k

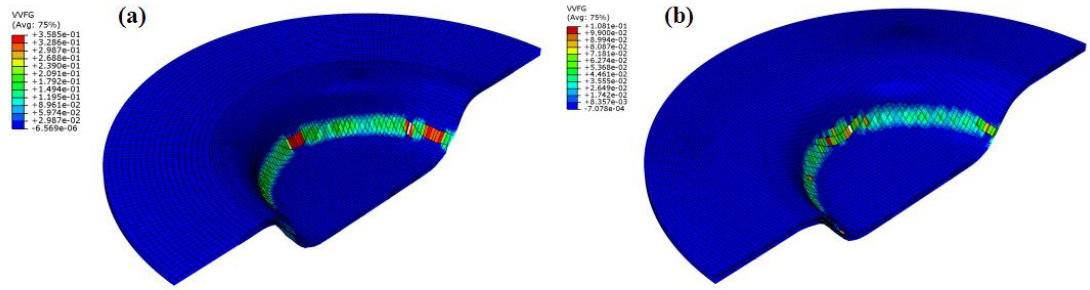


Fig. 14 void volume fraction due to growth at different temperatures: (a)423K, (b)298k

## 5. Conclusions

In this study, the formability of warm hydrodynamic deep drawing (HMDD) of AA2198-T3 Al-Li alloy through experimentation and finite element simulation was investigated. By using GTN model, a 3D FE model of the HMDD of A2198-T3 alloy sheets was developed at different temperatures. The effect of hydraulic pressure on HMDD process, formability and thickness distribution were studied. The main conclusions can be drawn as follows:

(1) It showed a very poor formability of AA2198-T3 Al-Li alloy at room temperature. The HMDD process with proper fluid pressure can improve the formability of the alloy. The formed depth promoted with the increase of hydraulic pressure. However, the fracture will occur after the pressure is up to a certain value at

room temperature.

(2) By utilizing the warm HMDD, the formability of AA2198-T3 Al-Li alloy was much improved at the elevated temperature (423 K). The hydraulic pressure has a significant influence on the warm HMDD. When the hydraulic pressure reached to a certain value (25 MPa), the plasticity can be much raised. Besides, the thickness distribution was more even at 423 K than the room temperature.

(3) By analyzing the SEM images, the brittle fracture of AA2198-T3 plays a main role at room temperature. The ductile fracture was shown at the elevated temperature. The GTN model can reflect the fracture behavior through calculating void nucleation, void growth, and void coalescence.

## Acknowledgement

The authors would like to acknowledge the key program supported by the Bureau of international cooperation of the Chinese Academy of Sciences (174321KYSB20150020), the National Natural Science Foundation of China (Grant No. 51605310), Jiangsu Province Science and Technology Program (Grant No. BE2016156), Shenyang Science and Technology Program (17-32-6-00), the Research Project of State Key Laboratory of Mechanical System and Vibration (MSV201708) and the Research Fund of Nanjing University of Aeronautics and Astronautics (No. YAH17019).

## References

[1] Abd El-Aty A, Xu Y, Guo XZ, Zhang S, Chen D (2017) Strengthening mechanisms, deformation behavior, and anisotropic mechanical properties of Al-Li alloys: A review. Journal of Advanced Research

[2] Rioja RJ, Liu J (2012) The Evolution of Al-Li Base Products for Aerospace and Space Applications. Metall. Trans. A 43(9): 3325-3337

[3] Zhang SF, Zeng WD, Yang WH, Shi CL, Wang HJ (2014) Ageing response of a Al–Cu–Li 2198 alloy. Mater. Des 63(2): 368-374

[4] Alexopoulos ND, Migklis E, Stylianos A, Myriounis DP (2013) Fatigue behavior of the aeronautical Al–Li (2198) aluminum alloy under constant amplitude loading. Int. J. Fatigue 56(11): 95-105

[5] Lequeu P, Lassince P, Warner T (2007) Aluminum Alloy Development for the Airbus A380 - part 2. Adv. Mater. Process 165(7): 41-44

[6] Decreus B, Deschamps A, Geuser FD, et al (2013) The influence of Cu/Li ratio on precipitation in Al–Cu–Li–x alloys. Acta Mater 61(6): 2207-2218

[7] Steglich D, Wafai H, Brocks W (2010) Anisotropic Deformation and Damage in Aluminum 2198 T8 Sheets. Int. J. Damage Mech 19(2): 131-152

[8] Palumbo G, Piglionico V, Piccininni A, et al (2015) Evaluation of the optimal working conditions for the warm sheet Hydroforming taking into account the yielding condition. Mater. Des 91: 411-423

[9] Prete AD, Papadia G, Vitis AD, Primo T (2011) Finite Element Simulations for Sheet Warm Hydroforming. AIP Conf. Proc 1353: 313-318

[10] Abd El-Aty A, Xu Y, Zhang SH, et al (2017) Experimental investigation of tensile properties and anisotropy of 1420, 8090 and 2060 Al-Li alloys sheet undergoing different strain rates and fibre orientation: a comparative study, Procedia Eng 207: 13-18

[11] Halkaci HS, Turkoz M, Dilmec M (2013) Enhancing formability in hydromechanical deep drawing process adding a shallow drawbead to the blank holder. J. Mater. Process. Technol 214(8): 1638-1646

[12] Kang BS, Ku TW (2011) Experimental study on multi-stage deep drawing for rectangular cup with high aspect ratio. Int. J. Adv. Manuf. Technol 53(1): 131-143

[13] Toros S, Ozturk F, Kacar I (2008) Review of warm forming of aluminum–magnesium alloys. J. Mater. Process. Technol 207(1-3): 1-12

[14] Hama T, Kitajima T, Nishimura Y, Fujimoto H, Takuda H (2012) Effect of Outflow Volume of Pressure Medium on liquid-Lubrication Effect during Sheet Hydroforming. Mater. Trans 53(5): 826-832

[15] Wang YM, Lang LH, Xie YS (2012) Numerical and Experimental Investigation into the Aluminum Alloy Irregular Box Sheet Hydroforming Process. Adv. Mater. Res 602-604: 1846-1849

[16] Koç M, Mahabunphachai S, Carsley JE (2010) Numerical and Experimental Investigations on Deformation Behavior of Aluminum 5754 Sheet Alloy under Warm Hydroforming Conditions. Numiform 1252(1): 107-115

[17] Hosseinpour M, Gorji A, Bakhshi M (2015) On the experimental and numerical study of formability of Aluminum sheet in warm hydroforming process. Modares Mechanical Engineering 7(3): 238-53

[18] Ling J, Guo XZ, Li HG (2015) Constitutive equation and numerical simulation of hydro-mechanical deep drawing of 2198 Al-Li alloy. Journal of Plasticity Engineering 22(2): 78-83

[19] Ludwik P (1909) Elemente der technologischen Mechanik[M]// Elemente der Technologischen Mechanik. Springer Berlin Heidelberg

[20] Alegre JM, Cuesta II, Bravo PM (2011) Implementation of the GTN Damage Model to Simulate the Small Punch Test on Pre-Cracked Specimens. Procedia Eng 10(1): 1007-1016

[21] Gurson AL (1977) Continuum Theory of Ductile Rupture by Void Nucleation and Growth: Part I-Yield Criteria and Flow Rules for Porous Media. J. Eng. Mater. Technol 99(1): 297-300

[22] Tvergaard V, Needleman A (1984) Analysis of the cup-cone fracture in a round tensile bar. Acta Metall 32(1): 157-169

[23] Benseddiq N, Imad A (2008) A ductile fracture analysis using a local damage model. Int. J. Press. Vessel. Pip 85(4): 219-227

[24] Fratini L, Lombardo A, Micari F (1996) Material characterization for the prediction of ductile fracture occurrence: An inverse approach. J. Mater. Process. Technol 60(1-4): 311-316

[25] Nègre P, Steglich D, Brocks W (2004) Crack extension in aluminium welds: a numerical approach using the Gurson-Tvergaard-Needleman model. Eng. Fract. Mech 71(16-17): 2365-2383

[26] Kami A, Dariani BM, Vanini AS, Comsa DS, Banabic D (2014) Numerical determination of the forming limit curves of anisotropic sheet metals using GTN damage model. J. Mater. Process. Technol 216: 472-483

# Figures

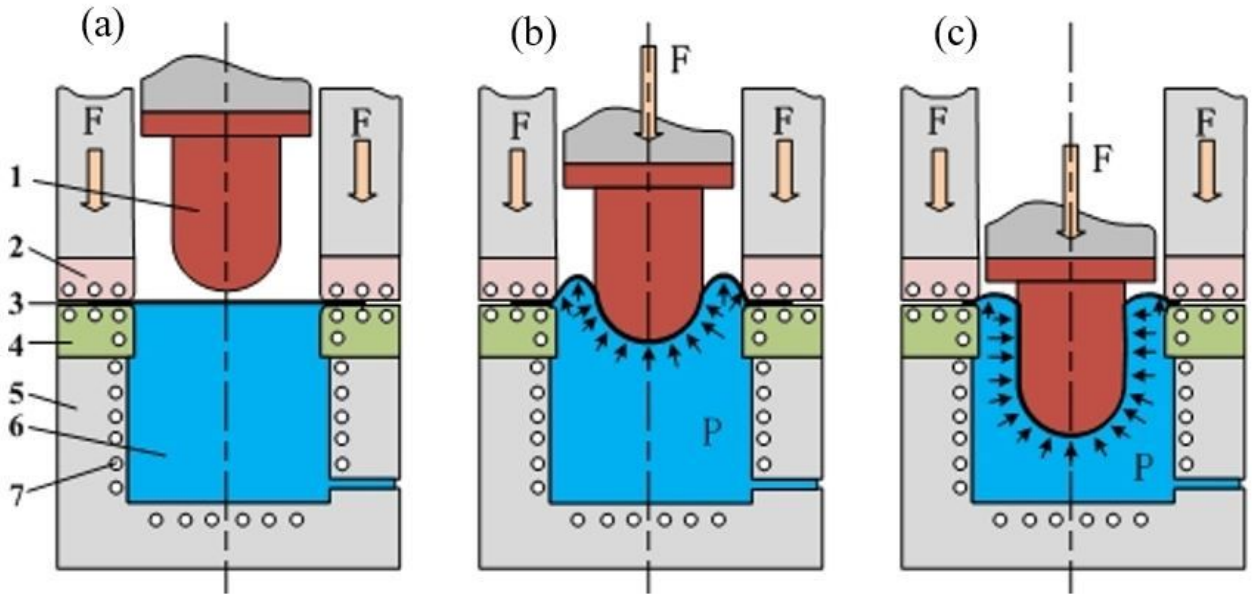


**Figure 1**

Schematic drawing of hydrodynamic deep drawing process: (a) Sheet in position and downward movement of blank holder; (b) Downward movement of punch; and (c) End of the sheet forming; 1-punch; 2-blank holder; 3-sheet; 4-die; 5-liquid cavity; 6-liquid; 7-electrical heat rod

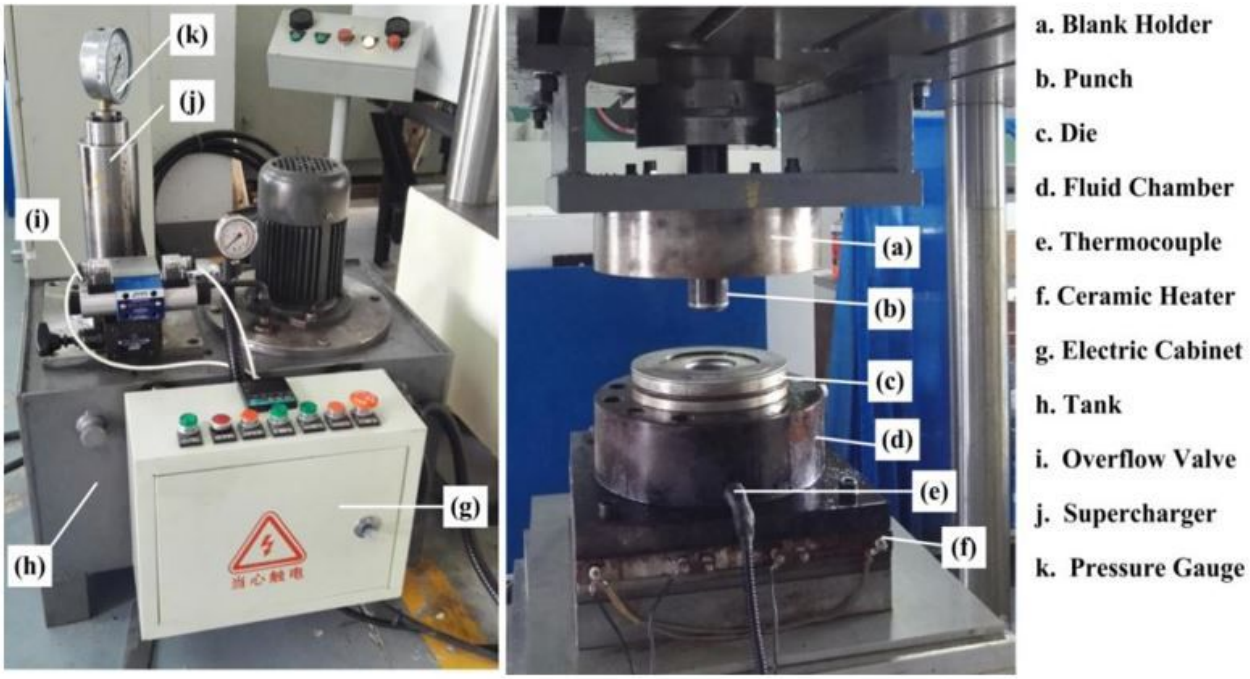

## Figure 2

The experiment equipment of the warm HMDD

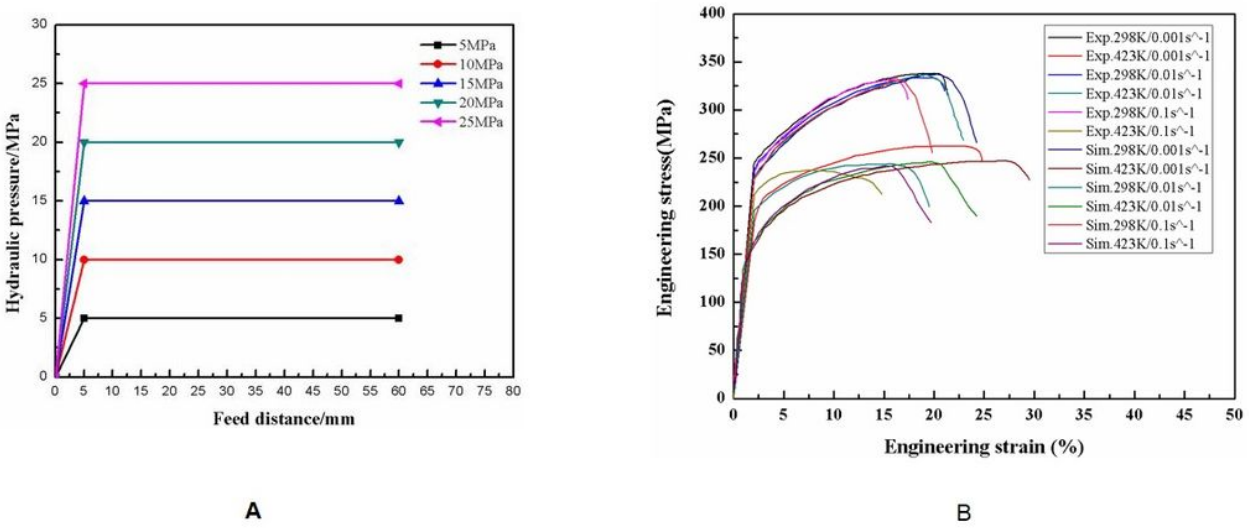


## Figure 3

a The loading paths of hydraulic pressures b Engineering stress-strain curves of AA2198-T3 Al-Li Alloy obtained from experiments and simulation

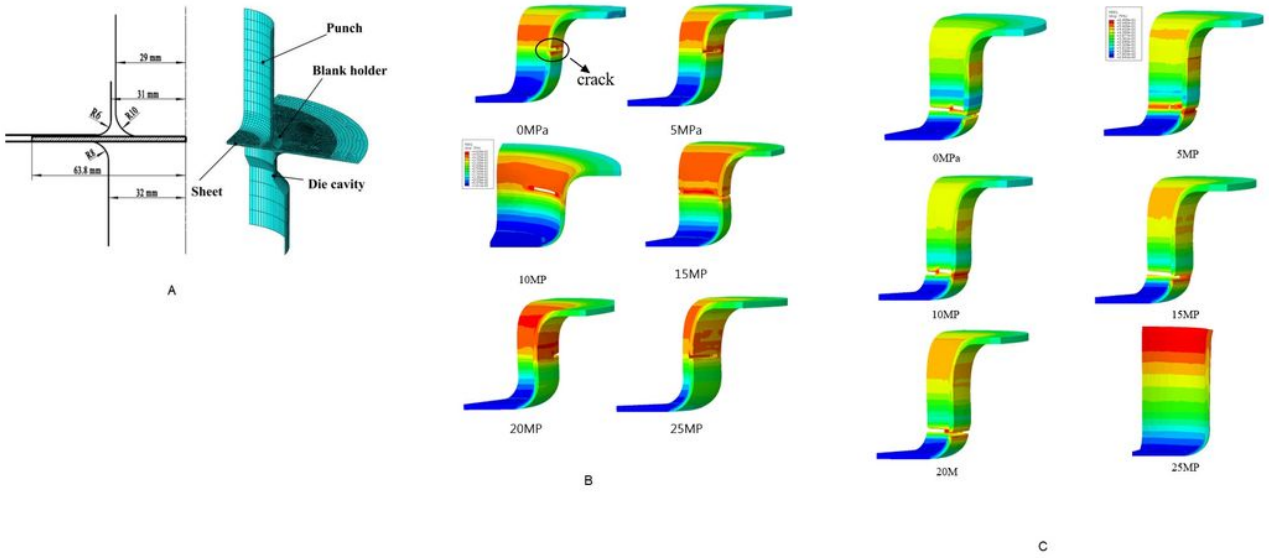


## Figure 4

a The finite element model and dimensions of tools. b Plastic strain distributions and fracture under different hydraulic pressures at 298K. c Plastic strain distributions and fracture under different hydraulic pressures at 423K.

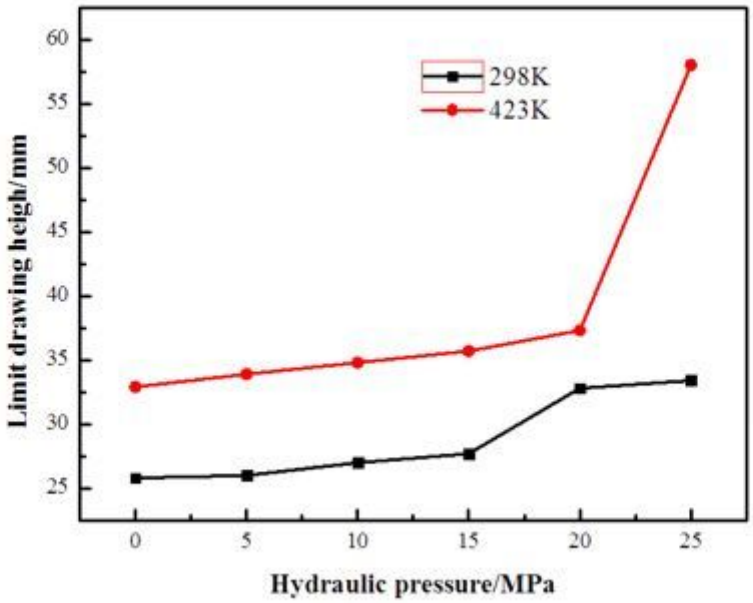


**Figure 5**

The limit drawing height at different hydraulic pressures.

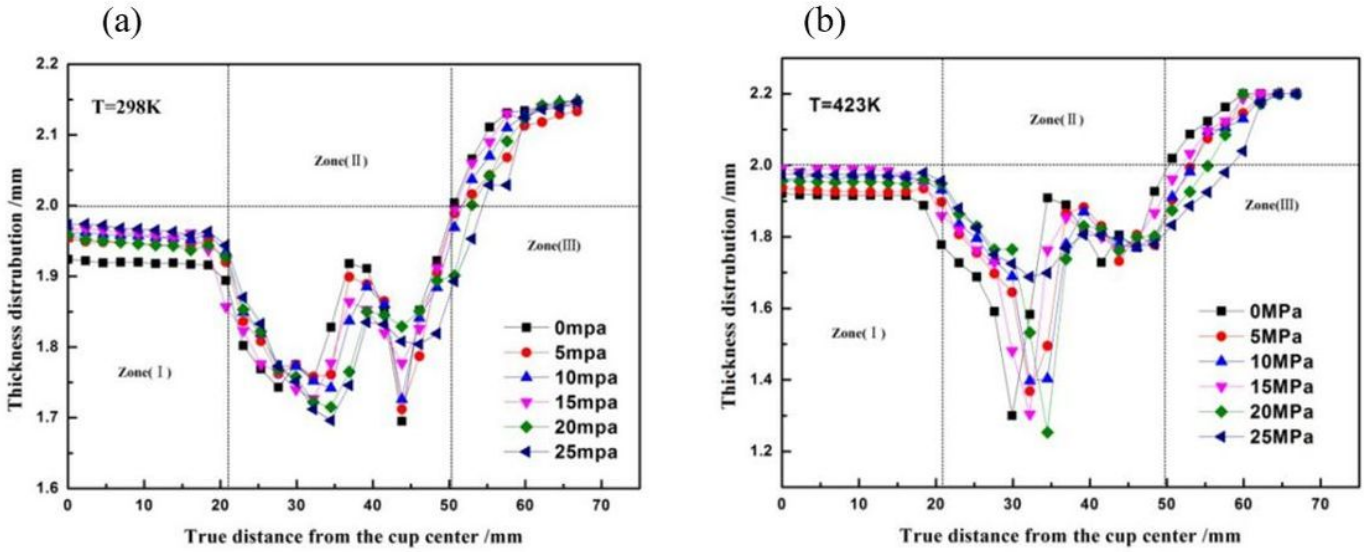


**Figure 6**

Thickness distribution of the formed parts achieved at the maximum height under different hydraulic pressures: (a) 298K, (b) 423K.

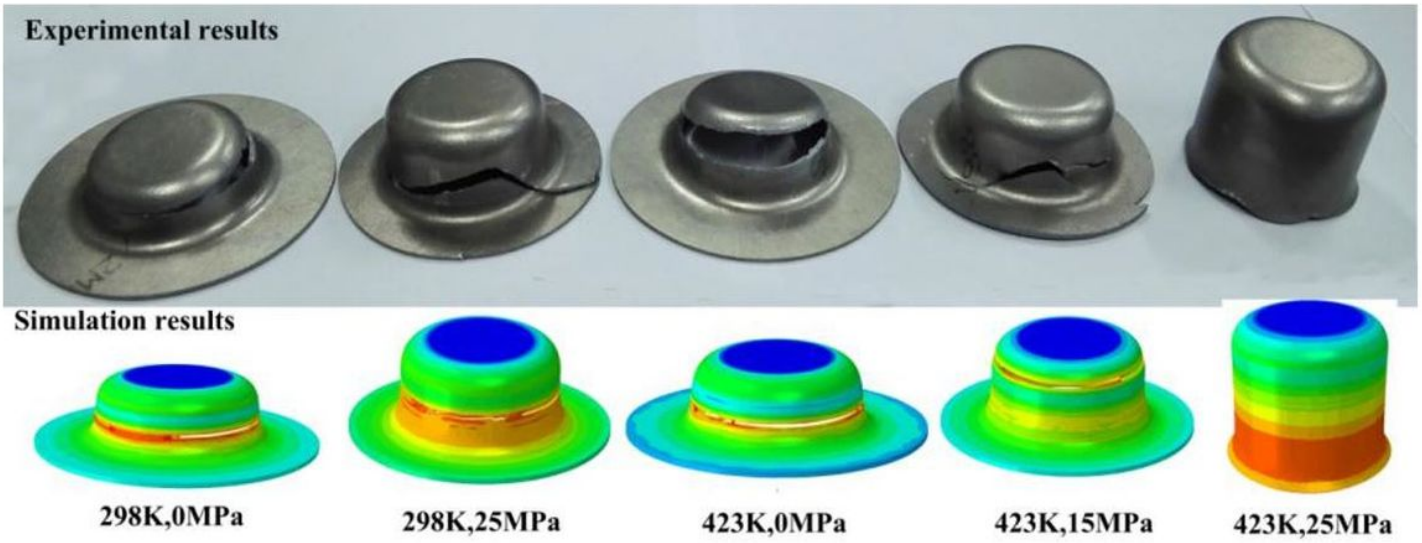


Figure 7

Comparison between experimental and simulation results.

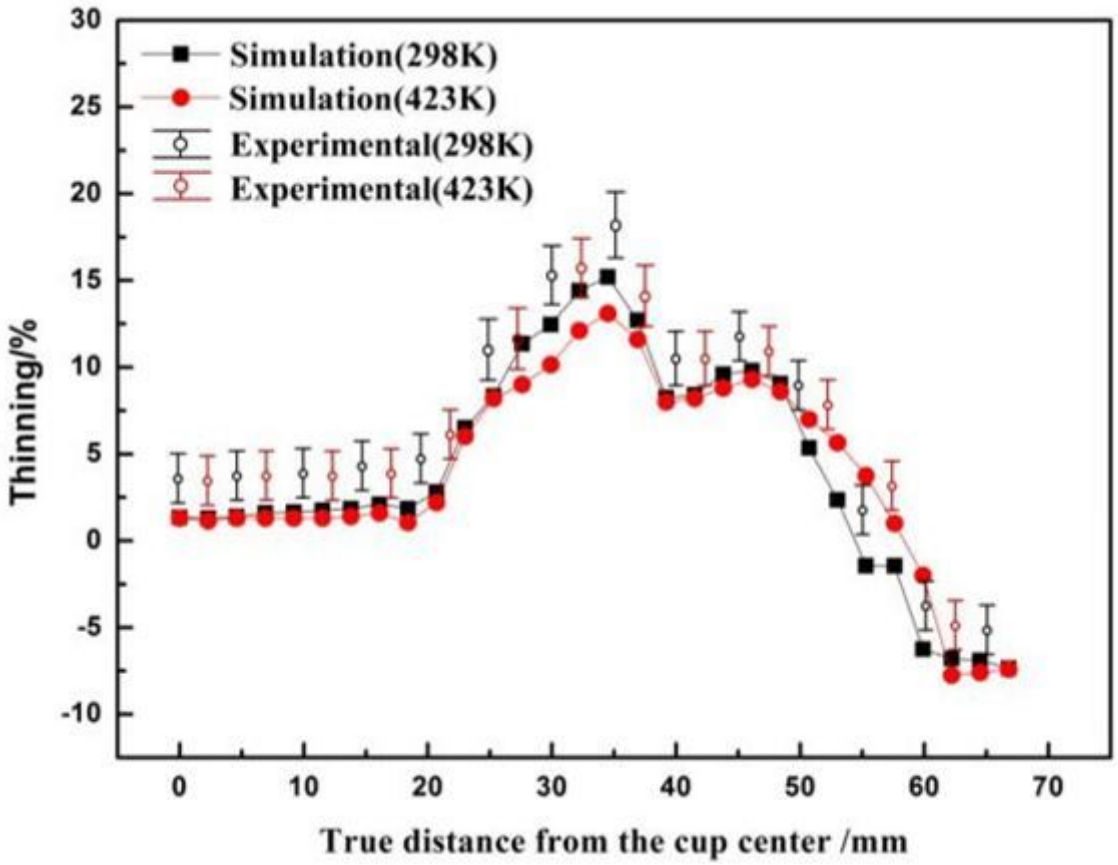


Figure 8

Thinning ratio of the formed part at the hydraulic pressure of 25 MPa

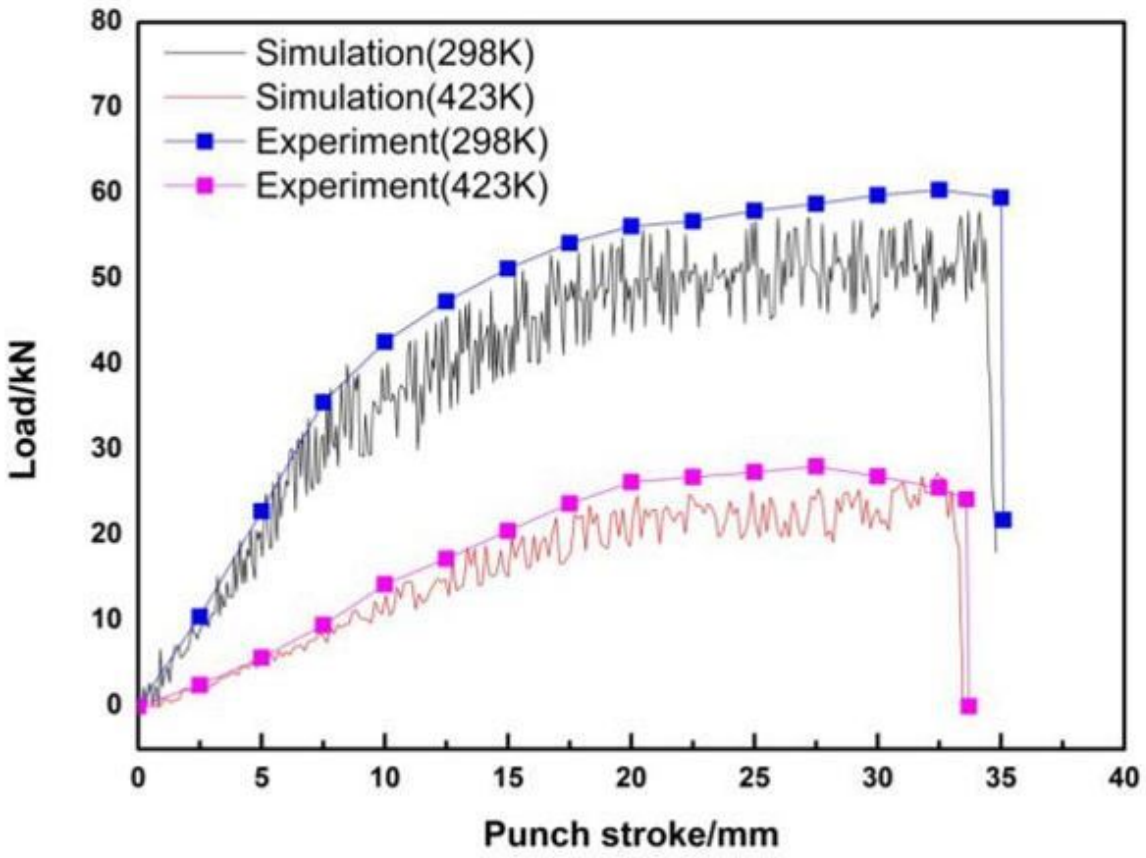


**Figure 9**

The comparison of punch force of simulation and experiment with the hydraulic pressure of 25 MPa

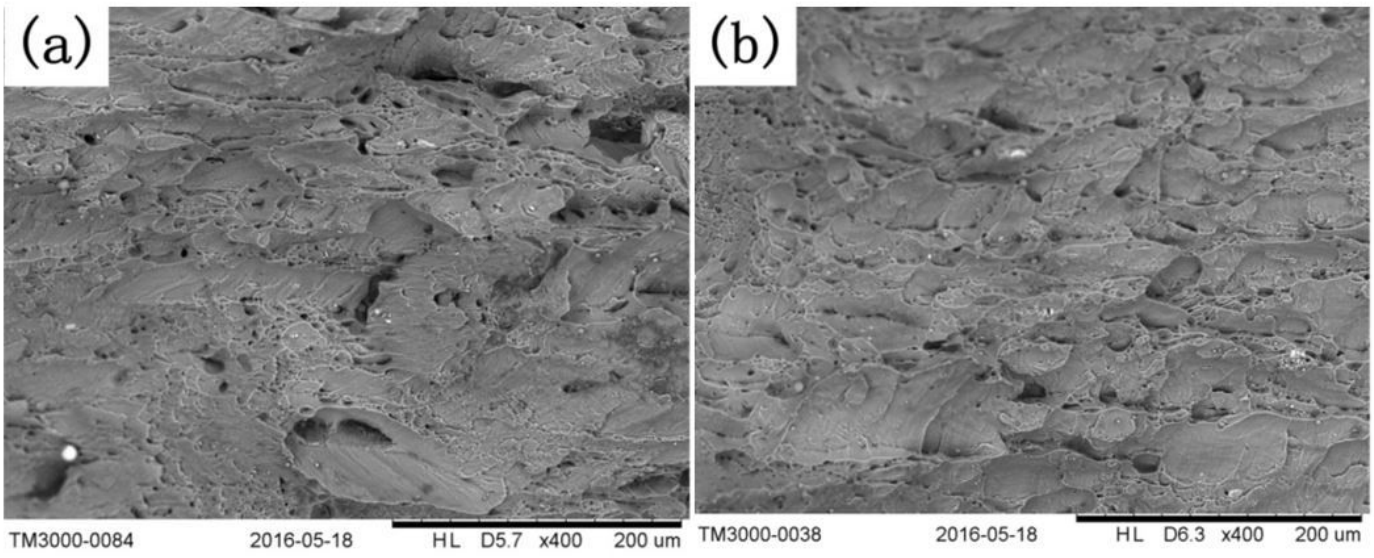


**Figure 10**

Fracture microstructure at low magnification (×400) in different temperatures: (a) 298K; (b) 423K

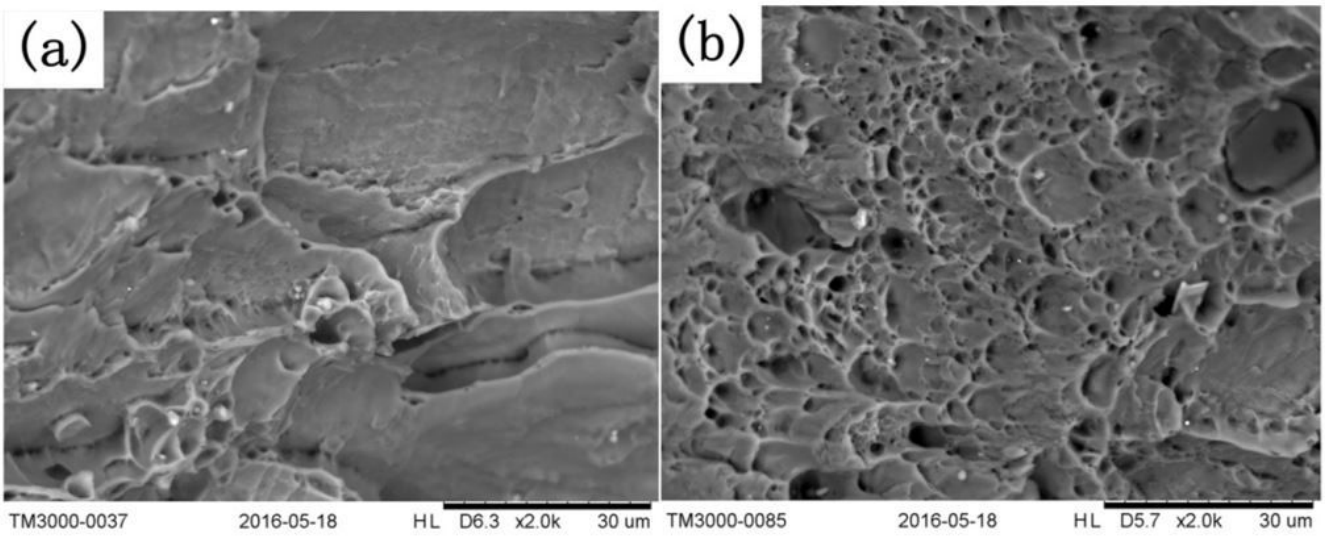


**Figure 11**

Fracture microstructure at high magnification (×2000) in different temperatures: (a) 298K; (b) 423K

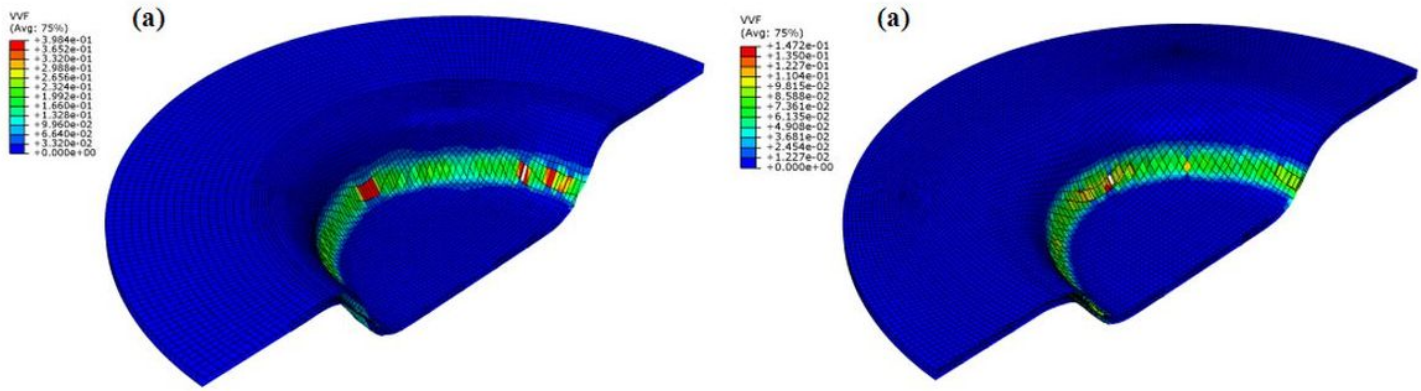


**Figure 12**

void volume fraction at different temperatures: (a) 423K, (b)298k

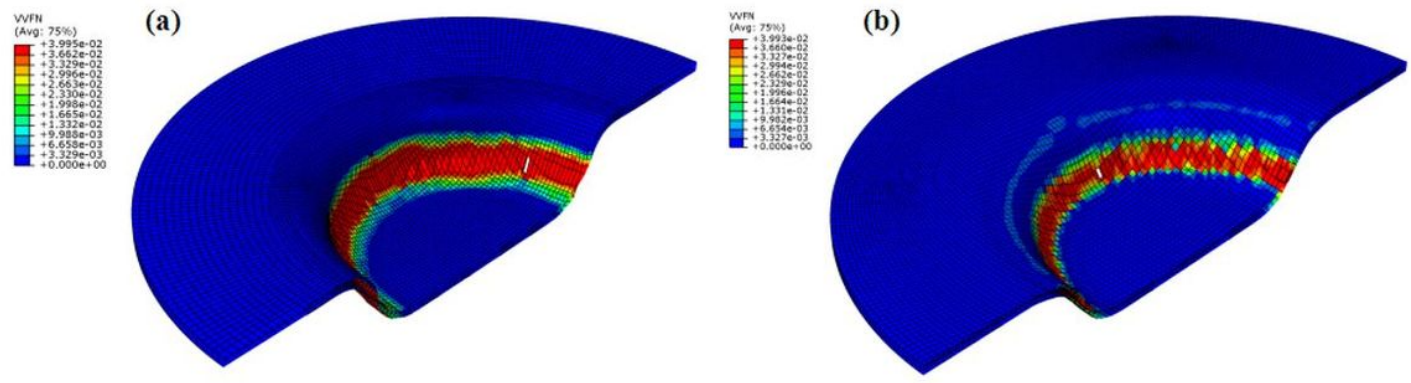


**Figure 13**

void volume fraction due to nucleation at different temperatures: (a)423K, (b)298k

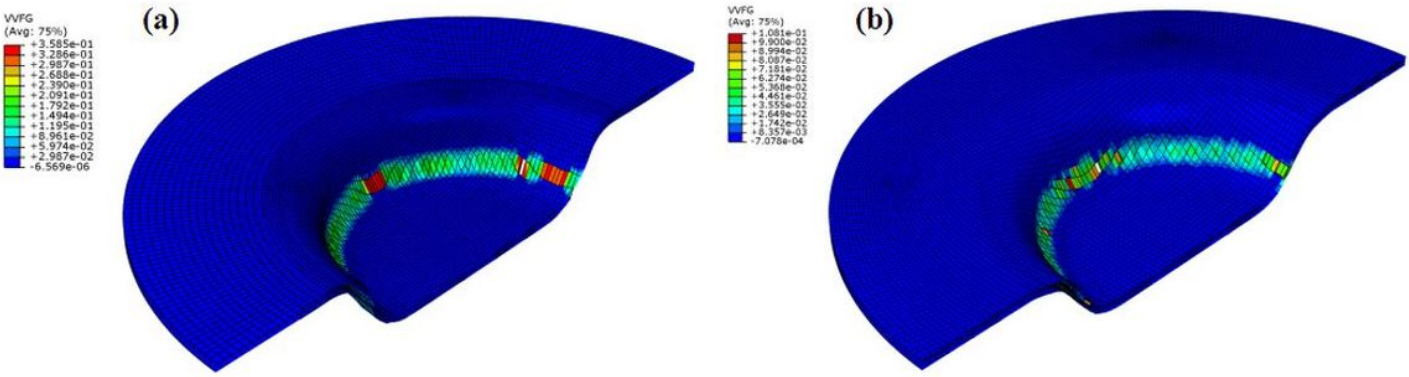


**Figure 14**

void volume fraction due to growth at different temperatures: (a)423K, (b)298k